

pubs.acs.org/JPCC Article

Surface Structure-Sensitive Enantioselectivity: Aspartic Acid Reaction Kinetics on All Surfaces Vicinal to Cu(111)

Carlos Fernández-Cabán and Andrew J. Gellman*



Cite This: https://doi.org/10.1021/acs.jpcc.1c01824



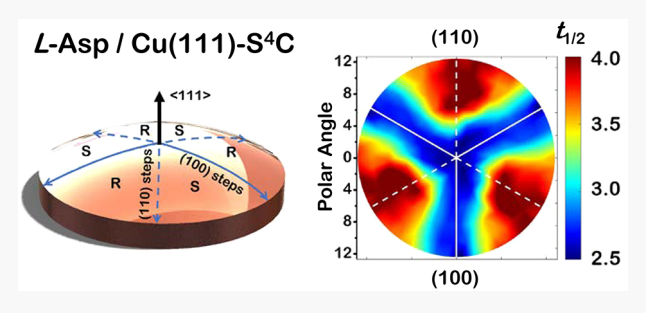
ACCESS

III Metrics & More

Article Recommendations

Supporting Information

ABSTRACT: Enantioselective reactions on chiral, single-crystal metal surfaces can provide novel insight into the origins of enantioselectivity in chiral molecular adsorption and catalysis. Using a high-throughput approach to study the surface of a spherical Cu single crystal, we have measured the surface reaction kinetics of aspartic acid decomposition on 169 different Cu(hkl) crystal planes vicinal to the Cu(111) orientation. These span both R- and S-surface chiralities comprehensively. The decomposition kinetics of D- and L-aspartic acids were measured and their decomposition rate constants were estimated on all 169 different surface orientations. The half-



times, $t_{1/2}^{(hkl)}$, for the decomposition of aspartic acid reveal that the reactivity for both enantiomers is lower along achiral directions exposing surfaces with (100) step edges than the reactivity along directions exposing surfaces with (110) step edges. The orientation-resolved rate constants, $k^{(hkl)}$, clearly reveal structure sensitivity on surfaces vicinal to Cu(111) but enantiospecificity is only observed for the initiation rate constant, $k_i^{(hkl)}$.

1. INTRODUCTION

One of the great challenges in the field of surface science and catalysis is understanding the influence of surface structure on reaction kinetics. The best-known example of surface structure sensitivity is the rate-limiting step in ammonia synthesis, that is, N₂ dissociation on single crystalline Fe surfaces, the primary catalyst for ammonia synthesis from N2 and H2. The rate of N2 dissociation differs between the three low-Miller-index planes of iron, $Fe(111) \gg Fe(100) > Fe(110)$, consistent with independent measurements of the relative kinetics of highpressure ammonia synthesis on these three surfaces. 1,2 Understanding the relationship between surface reaction kinetics and surface structure at a predictive level is of critical importance in the optimization of catalytic processes and the design of new catalysts. The work presented herein studies what is perhaps the subtlest form of surface structure sensitivity or chemical selectivity, namely, the enantioselectivity of the reactions of chiral molecules on intrinsically chiral surfaces. In this case, enantioselectivity is dictated solely by the diastereomeric structural relationship between the chiral adsorbate and the chiral surface.^{3,4}

The societal importance and relevance of molecular chirality arise from the fact that biomolecules such as proteins, sugars, amino acids, and DNA are chiral. One of the interesting features of living organisms is that their biomolecules are homochiral, meaning that life only uses one of their two possible enantiomers. Because human physiology is homochiral, when synthetic chiral compounds such as pharmaceuticals are ingested as racemic mixtures, one enantiomer can have vastly different physiological activity than the other. As a consequence,

all chiral pharmaceuticals must be produced in enantiopure form using enantioselective chemical processes.⁵ Enantioselective chemical processes require chiral media such as surfaces, catalysts, or solvents to differentiate the enantiomers of reactants, intermediates, and products. Chiral surfaces are good candidates for the development and understanding of enantioselective processes because surfaces play a crucial role in chemical processes such as adsorption, catalysis, and crystallization. One of the challenges to optimizing enantioselective processes on chiral surfaces is that it requires a fundamental understanding of their enantiospecific interactions with chiral molecules.3,6,7 Fundamentally, this is a problem in surface structure sensitivity. Optimization of enantioselective processes on chiral surfaces requires an understanding of the effect of surface structure on reaction kinetics. Because of the infinite number of possible surface orientations and structures, a highthroughput approach is needed to comprehensively study the kinetics of enantioselective reactions on chiral surfaces of different crystallographic orientations. This study demonstrates a method for measurement of enantiospecific reaction kinetics of a chiral molecule on Cu metal surfaces across a continuous distribution of crystal plane orientations.^{8,9}

Received: February 28, 2021 Revised: April 12, 2021



Many chiral surfaces are made by adsorption of chiral molecules onto achiral surfaces. The chiral modifier imparts chirality to the surface by breaking the structural symmetry of the achiral surface, rendering it chiral.⁶ Some inorganic materials such as quartz and intermetallic compounds such as GaPd have chiral bulk structures and, therefore, they expose chiral surfaces.^{3,10} Somewhat counterintuitively, chiral surfaces can also be obtained from materials with achiral bulk structures, e.g., pure metals. Such surfaces are intrinsically chiral and can be obtained by cleaving the bulk metal lattice along a low-symmetry plane. For face centered cubic (FCC) metals, a surface is achiral if any two of its Miller indices (hkl) are equal to one another or if any of them are zero. Consequently, an FCC(hkl) surface is chiral if $h \neq k \neq l \neq h$ and $h \times k \times l \neq 0$. The ideal structures of chiral metal surfaces have low-Miller-index terraces separated by kinked monoatomic step edges. These structures differ in terms of which low-Miller-index facets form the terraces, the straight portions of the step edges, and the kinks (Section SI 1). 14 At a finer level of detail, these chiral surfaces vary in terms of the spacing between steps separating the terraces and the spacing between the kinks along the step edges. These types of intrinsically chiral metal surfaces have been shown to exhibit enantiospecific interactions with a variety of chiral adsorbates.^{3,15–19}

One challenge to understanding the effect of chiral surface structures on enantioselectivity is the infinite number of possible surface orientations that can be obtained from any bulk crystal structure. The stereographic triangle is a two-dimensional (2D) map of all possible surfaces that can be obtained from a given bulk structure, as shown in Section SI 2. The points inside the stereographic triangle represent chiral surfaces. 20 Studying the structure sensitivity of surface reaction kinetics is a challenge because of the infinite number of possible surface orientations; however, addressing this challenge provides an opportunity to obtain a comprehensive understanding of surface structure sensitivity, in general. Most surface science studies have examined achiral low-Miller-index surfaces, and comparatively little attention has been given to high-Miller-index chiral surfaces that contain steps and kinks. One limitation of previous studies is that they tackle one surface at a time, i.e., they study one single point in the stereographic triangle. The key aspect of this study is that it circumvents this limitation and examines 169 surface orientations concurrently.

The barrier to comprehensive study of structure sensitivity across surface orientation space can be circumvented by using curved single-crystal samples called surface structure spread single crystals (S⁴C) that expose continuous distributions of surface orientations (Figure 1).21 S4Cs span a continuous portion (2D area) of the stereographic triangle. They allow us to study many surface orientations under identical experimental conditions. Figure 1A shows a graphic illustration of a Cu(111) $\pm 14^{\circ}$ -S⁴C. The curved face of the Cu disk is spherical with a 21 mm radius of curvature. The (111) plane is located at the top and center points of the dome, and the curvature spans all possible surface orientations lying within 14° of the [111] orientation. Six high-symmetry directions divide the curved surface into six regions. These regions are arranged around the (111) pole and contain surface orientations with R- and Schiralities, alternating as one goes around the (111) pole. The points along the solid blue lines expose achiral surfaces with (111) terraces separated by (100) steps (see Section SI 2). The points along the dashed blue lines expose achiral surfaces with (111) terraces separated by (110) steps. The step density

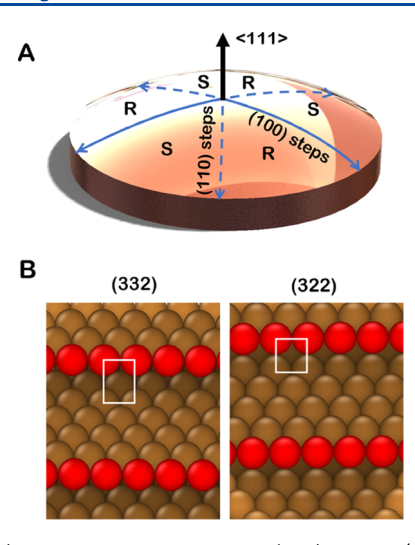


Figure 1. (A) Graphic illustration of a Cu(111) \pm 14°-S⁴C (10 mm in diameter \times ~2 mm thickness). The achiral (111) plane is at the center point. The points along the solid blue lines expose achiral surfaces with (111) terraces and (100) steps. The points along the dashed blue lines expose achiral surfaces with (111) terraces and (110) steps. The sample has six regions of alternating chirality. (B) Illustrations of the ideal achiral Cu(332) and Cu(322) surfaces. Both of these surfaces are exposed at the edge of the Cu(111) \pm 14°-S⁴C sample. These structures have (111) terraces separated by monoatomic step edges. Cu(332) has (110) steps and Cu(322) has (100) steps.

increases continuously from the (111) center point to the edges of the S⁴C. At the edges, the terrace widths are ~1 nm. The surfaces on the edges of the Cu(111) \pm 14°-S⁴C have (111) terraces that are ~5 closed-packed rows in width separated by monoatomic step edges. The steps formed by either (100) or (110) microfacets are shown in Figure 1B. The use of a S⁴C coupled with spatially resolved experimental techniques allows the study of enantiospecific surface reaction kinetics across a continuous distribution of surface orientations. In this work, we use a high-throughput methodology to measure isothermal rate constants for the decomposition of both D- and L-aspartic acids (Asp, HO₂CCH(NH₂)CH₂CO₂H) on 169 Cu(hkl)^{R&S} surface orientations vicinal to the (111) plane.

One of the advantages of using the S⁴Cs for high-throughput measurements of surface reaction kinetics is that they allow the study of a continuous distribution of different surface structures, all treated using the same experimental conditions and having the same history. All points on the sample surface are subjected to the same exposure of Asp, temperature cycling, and analysis conditions. This minimizes random errors introduced into a large set of experiments conducted on many discreet single crystals having different surface orientations. Prior work by us studied the decomposition kinetics of D-tartaric acid (D-TA, HO₂CCH(OH)CH(OH)CO₂H) on a Cu(110)-S⁴C.⁸ That work identified the surface orientations around Cu(14,17,2)^{R&S} as exhibiting a clear maximum in enantioselectivity between Rand S- surface orientations. Herein, we extend the protocols used in that prior work on TA surface chemistry to a study of Asp surface chemistry. The data presented herein constitutes the most comprehensive data set yet obtained that compares the surface reaction kinetics of both enantiomers of a chiral compound on a continuous range of surface orientations.

Asp is an interesting chiral probe because its decomposition mechanism and kinetics on Cu single-crystal surfaces are well understood. ^{22–24} At saturation coverage, Asp adsorbs on Cu

surfaces at 400 K as a doubly deprotonated aspartate species (-O₂CCH(NH₂)CH₂CO₂-). During heating, adsorbed Asp decomposes stoichiometrically to H2, 2CO2, and acetonitrile (N≡CCH₃), all of which desorb from the surface. Regiospecific isotope labeling of Asp with ¹³C has shown that cleavage of the 3C-4C bond proceeds first to yield one CO₂ molecule followed by 1C-2C cleavage to yield the other CO₂. The acetonitrile comes from the interior 2C-3C atoms. More importantly, Asp decomposes via an autocatalytic mechanism called a vacancymediated, surface explosion reaction. 22,25 A surface explosion occurs when the adsorbate requires an adjacent vacancy to decompose. Initially, an adsorbate in a saturated monolayer, θ_{Asp} = 1, desorbs or decomposes without the requisite vacancy. This is referred to as an initiation or nucleation step and results in the creation of a vacancy. The creation of an initial vacancy then opens a low barrier pathway to further decomposition of Asp adsorbates. A neighboring Asp species then uses the adjacent vacancy to decompose, creating two vacancies. Two adsorbates adjacent to those vacancies then decompose and thereby create four vacancies. The areal density of vacancies thereby increases exponentially with time leading to an autocatalytic acceleration of the rate even under isothermal conditions. 26,27 The model describing surface explosions yields the rate law for the autocatalytic process as a function of the adsorbate coverage, θ , and the vacancy concentration, $(1-\theta)$. The rate law that best describes the kinetics of Asp decomposition on Cu by a surface explosion is

$$r = -\frac{\mathrm{d}\theta_{\mathrm{Asp}}}{\mathrm{d}t} = k_i \theta_{\mathrm{Asp}} + k_e \theta_{\mathrm{Asp}} (1 - \theta_{\mathrm{Asp}})^2 \tag{1}$$

This rate law contains an initiation rate constant, k_p and an explosion rate constant, k_e . The exponent in the explosion term describes the order of the reaction with respect to the vacancy concentration. The fact that it is second-order suggests that two adjacent vacancies are needed for decomposition of adsorbed Asp. The same second-order dependence on vacancy coverage has been observed for TA decomposition. These nonlinear reaction kinetics can result in highly enantiospecific reaction rates on chiral Cu surfaces. 16,22

Because both Asp and most of the Cu surfaces on the $Cu(111) \pm 14^{\circ}$ -S⁴C are chiral, the Asp decomposition process has the potential to cast light onto the fundamental origins of enantioselectivity and its dependence on surface orientation. One of the challenges of studying enantioselectivity is that it is perhaps the most subtle form of chemical selectivity. The energy differences that give rise to enantioselectivity between pairs of enantiomers tend to be on the order of only a few kJ/mol. For example, the enantiospecific difference between the energies for equilibrium adsorption of D- and L-Asp on Cu(3,1,17)^{R&S} surfaces is just 3.2 kJ/mol, i.e., roughly equal to k_BT at the temperatures at which Asp decomposes in the experiments described herein.²¹ Accurate measurement of the small differences in reaction kinetics between enantiomers remains challenging but is critical for the optimization of enantioselective reactions on chiral surfaces.

2. EXPERIMENTAL SECTION

2.1. S⁴**C Preparation.** The $Cu(111) \pm 14^{\circ}$ -S⁴C was prepared from a commercially available Cu(111) single crystal (Monocrystals Inc.), which was 10 mm in diameter and 2 mm in thickness. The Cu(111) single-crystal disc with a flat surface was nanomachined using single-point diamond turning (SPDT) by a

commercial provider (Empire Precision Plastics, Rochester, NY) rendering the surface curved. The final shape was a section of a 21 mm radius spherical dome (Figure 1). This was vacuum-braised to a $14 \times 14 \times 3$ mm³ Cu block so that the sample could be mounted in the sample holder without direct handling. The sample surface was then cleaned in ultrahigh vacuum by 1.0 keV Ar $^+$ sputtering and annealing cycles at 900 K until the surface was sufficiently clean and ordered that it yielded an low-energy electron diffraction (LEED) pattern.

Electron backscattered diffraction shown in Section SI 3 was used to determine the rotational orientation of the Cu lattice vectors. Pole figures were obtained from electron backscatter diffraction from the Cu(111) \pm 14°-S⁴C. The (111) pole is located at the center point of the sample. The orientations of the (100) and (110) poles are indicated and determine the orientation of the bulk lattice vectors.

2.2. Asp/S⁴C Surface Preparation. Asp adsorption and decomposition on the Cu(111) \pm 14°-S⁴C were studied in a ThetaProbe. This apparatus has a preparation chamber and an analysis chamber. The preparation chamber is equipped with a homemade sublimation source for Asp deposition onto the surface and a sputter ion gun to clean the surface. The analysis chamber is equipped with a focused and monochromated X-ray source and a hemispherical energy analyzer to perform spatially resolved X-ray photoelectron spectroscopy (SR-XPS). Prior to the study of Asp decomposition kinetics on its surface, the $Cu(111) \pm 14^{\circ}-S^{4}C$ sample was cleaned in the preparation chamber using Ar⁺ ion sputtering followed by annealing at 900 K for 5 min. Asp was then adsorbed on the surface from the sublimation source held at ~435 K. A saturated monolayer of Lor D-Asp was adsorbed with the surface temperature held at 400 K and exposed to the L- or D-Asp flux for 20 min. At a surface temperature of 400 K, a saturated monolayer of Asp in the form of aspartate was formed with no multilayer formation.²² In this work, the fractional saturation coverage at any point on the surface was normalized to the initial coverage of $\theta_{Asp}^{(hkl)}(0) = 1$.

2.3. SR-XPS Analysis. The spatiotemporal evolution of the local Asp coverage, $\theta_{\rm Asp}^{(hkl)}(t)$, across the Cu(111) \pm 14°-S⁴C was measured using SR-XPS. After first adsorbing the Asp monolayer, the O 1s XPS signal was measured on a circular grid of 169 points (see Section SI 4). The sample was then heated isothermally at 433 K for a series of varying time intervals and then quenched before measuring the O 1s XPS signals at all points on the grid. Each annealing and quenching step consisted of heating the sample at 1 K/s from ~305 to 433 K, holding the temperature at 433 K for the prescribed period of time (30-1200 s), and then cooling at \sim -1 K/s to <390 K before using O 1s SR-XPS to measure the local coverage of Asp remaining at each point on the surface. The heating schedule is indicated by the hash marks showing the quench times on top of Figure 2. A set of 70 heating periods totaling 7415 s were used to completely decompose the original Asp monolayer at all points on the $Cu(111) \pm 14^{\circ}-S^{4}C.$

To determine the local coverage of Asp after each annealing and quenching step, O 1s XPS spectra were collected at 169 points distributed evenly about concentric circles spaced at multiples of 0.75 mm in radial distance from the center of the Cu(111) \pm 14°-S⁴C, as shown in Section SI 4. SR-XPS was conducted using an X-ray spot diameter of 400 μm . This corresponds to a spread of ~1° in surface orientation over the sampled region of the Cu(111) \pm 14°-S⁴C. Collection of the O 1s XPS spectra required 19 s per point on the S⁴C. The decomposition of Asp on Cu surfaces results in the desorption of

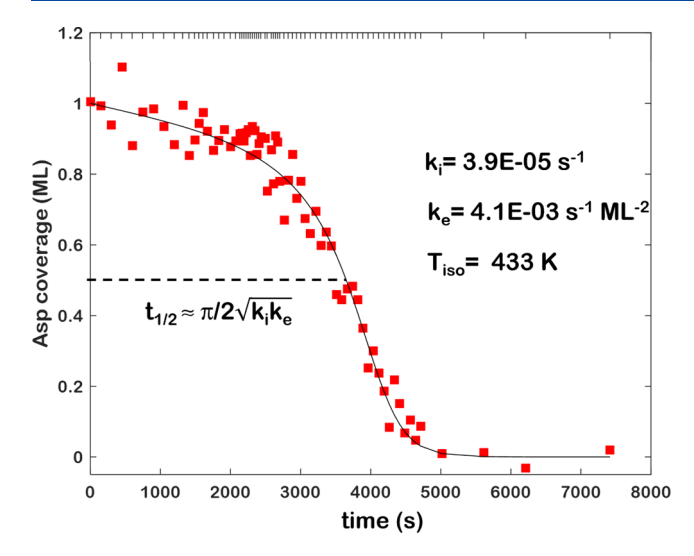


Figure 2. L-Asp coverage versus time (red squares) at $T_{\rm iso} = 433$ K measured at the (111) center point of the Cu(111) \pm 14°-S⁴C. The fit of the rate law for L-Asp decomposition (eq 1) to the data is represented by the solid black curve. The fit is parameterized by $k_i^{(111)}$ and $k_e^{(111)}$. The time intervals used to monitor $\theta_{\rm Asp}^{(hkl)}(t)$ at all 169 points on the Cu(111) \pm 14°-S⁴C are indicated by the hash marks on top of the plot.

CO₂, H₂, and CH₃C \equiv N leaving no decomposition products adsorbed on the surface at an extent of reaction of EOR = 100%. The time-dependent coverage of Asp at each point, \vec{r}_{hkl} , on the sample, $\theta_{\rm Asp}^{(hkl)}(t)$, was estimated using the O 1s XPS signal intensity. By using the initial O 1s signal intensity of the Asp monolayer at point \vec{r}_{hkl} , $I_{\rm O \, 1s}^{(hkl)}(0)$, and the O 1s intensity after the reaction was completed, $I_{\rm O \, 1s}^{(hkl)}(\infty)$, the Asp coverage at all intervening times was estimated using eq 2

$$\theta_{\text{Asp}}^{(hkl)}(t) = \frac{I_{\text{Ols}}^{(hkl)}(t) - I_{\text{Ols}}^{(hkl)}(\infty)}{I_{\text{Ols}}^{(hkl)}(0) - I_{\text{Ols}}^{(hkl)}(\infty)}$$
(2)

3. RESULTS

The surface decomposition kinetics of adsorbed Asp were studied at T_{iso} = 433 K using time-resolved SR-XPS, as described

above. The local coverages of D- and L-Asp were monitored at 169 points across the Cu(111) \pm 14°-S⁴C as a function of time, $\theta_{\text{Asp}}^{(hkl)}(t)$. The L-Asp coverage versus time, $\theta_{\text{L-Asp}}^{(111)}(t)$, at the Cu(111) point of the Cu(111) \pm 14°-S⁴C is shown in Figure 2. The hash marks on top of the figure indicate the times at which the sample temperature was quenched during heating at 433 K. After each quenching step, SR-XPS was used to map the local coverage across the $Cu(111) \pm 14^{\circ}$ -S⁴C. The slow initiation process is observable from t = 0 to 2500 s. The explosive autocatalytic acceleration of the decomposition rate follows from t = 2500 to 4500 s, as indicated by the rapid decay in L-Asp coverage. Following the explosion and depletion of the adsorbed L-Asp, $\theta_{\text{\tiny L-Asp}}^{(111)}$ goes to zero. Similar initiation and explosion features are also observed in the coverage decay curves obtained from the other 168 surface orientations sampled on the Cu(111) $\pm 14^{\circ}$ -S⁴C. One feature of these curves that is particularly easy to measure with high accuracy is the half-time, $t_{1/2}^{(hkl)}$, needed to reach a coverage of $\theta_{\text{L-Asp}}^{(hkl)}(t_{1/2}) = 0.5$. The values of $t_{1/2}^{(hkl)}$ measured from the sampled surface orientations span the range $t_{1/2}^{(hkl)} = 2320-4160$ s. The fit of the L-Asp decomposition rate law (eq 1) to the measured data for $\theta_{\text{L-Asp}}^{(111)}(t)$ is shown by the black curve in Figure 2. The optimal fit yields estimates of $k_i^{(111)}$ = 3.9 \pm 0.5 \times 10⁻⁵ s⁻¹ and $k_e^{(111)}$ = 4.1 \pm 0.5 \times 10⁻³ s⁻¹ ML_v⁻², where $\mathrm{ML_v}$ is the unit of vacancy coverage. All surface orientations exhibit $k_e^{(hkl)} \gg k_i^{(hkl)}$. This has also been observed in the case of TA decomposition on a $Cu(110) \pm 14^{\circ}$ -S⁴C.⁸ The analytical solution of eq 1 allows us to express various features of the coverage decay curves, $\theta_{i\text{-Asp}}^{(hkl)}(t)$, in terms of $k_e^{(hkl)}$ and $k_i^{(hkl)}$. Given the condition that $k_e^{(hkl)} \gg k_i^{(hkl)}$, it is easy to show that $t_{1/2} \cong \pi/2\sqrt{k_i k_e}$. The relationship between $t_{1/2}$ and $k_i \cdot k_e$ is useful because it will serve as a metric for the enantiospecificity of the decomposition kinetics. It is also the case that the nature of the solution to eq 1 allows high accuracy estimates of $t_{1/2}$ from the fits to the $\theta_{\text{L-Asp}}^{(hkl)}(t)$ data. ²⁸

In addition to the quenching measurement made on 169 different points, the time-dependent coverages of L-Asp were measured continuously (no quenching) at an isothermal temperature of 425 K on seven different Cu(hkl) surfaces vicinal to the (111) plane. Figure 3A shows a map of the seven points studied on the Cu(111) \pm 14°-S 4 C. These surfaces lie in a region of the Cu(111) \pm 14°-S 4 C having R-chirality. Using a

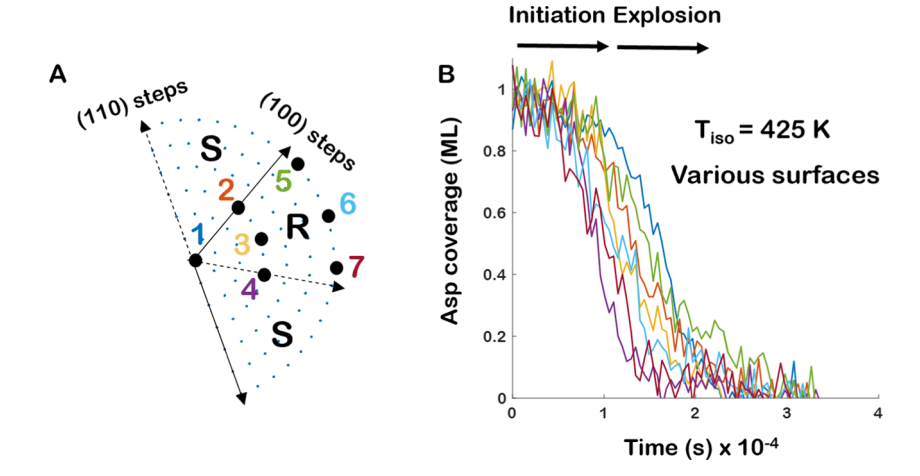


Figure 3. (A) Map of the seven points across the Cu(111) \pm 14°-C⁴C sample at which L-Asp decomposition was measured continuously at $T_{\rm iso}$ = 425 K using O 1s XPS. These points are indicated on the grid of 169 points used for subsequent experiments at $T_{\rm iso}$ = 433 K with periodic quenching. (B) Plots of $\theta_{\rm L-Asp}(t)$ during decomposition at $T_{\rm iso}$ = 425 K at the seven points indicated on the map in (A). The temporal evolution of the L-Asp coverage was estimated from the O 1s XPS data collected at each of the seven points.

The Journal of Physical Chemistry C

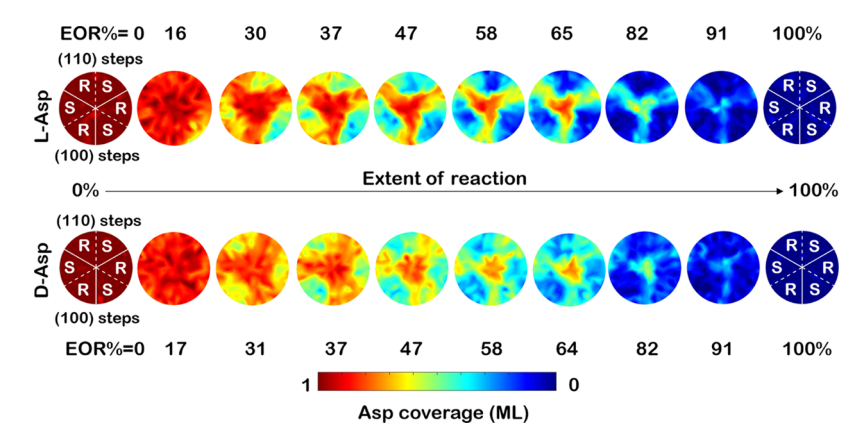


Figure 4. L-Asp (top) and D-Asp (bottom) coverage maps, $\theta_{\rm Asp}^{(hkl)}(t)$, versus EOR during isothermal decomposition at 433 K on the Cu(111) \pm 14°-S⁴C. The coverage was obtained using the O 1s XPS signal measured on a grid of 169 points spanning the inner \pm 12.4° of the Cu(111) \pm 14°-S⁴C. The extent of reaction (EOR) for the decomposition of both enantiomers after having annealed for a given time, t, was estimated using the average value of $\theta_{\rm Asp}^{(hkl)}(t)$ remaining on the surface. The evolution of the coverage decay reveals a 3-fold rotational symmetry for both enantiomers about the Cu(111) center point. The maps for the decomposition of each Asp enantiomer represent 10 of 70 in the complete data set (see Section SI 6).

procedure different from the heating and quenching experiments of Figure 2, this experiment first saturated the surface with L-Asp and then heated the sample to $T_{\rm iso}=425$ K and held it there while obtaining O 1s XP spectra from each of the seven points. Figure 3B shows the L-Asp coverage decay curves, $\theta_{\rm L-Asp}^{(lkl)}(t)$, during isothermal decomposition at 425 K on the seven different Cu(hkl) surfaces. The values of $\theta_{\rm L-Asp}^{(hkl)}(t)$ were estimated using eq 2. The data reveal (Section SI 5) that the rate constants for both the initiation process, $k_i^{(hkl)}$, and explosion process, $k_e^{(hkl)}$, span a range of $\sim 3\times$.

The coverage maps, $\theta_{\rm Asp}^{(hkl)}(t)$, obtained at all 169 points during D- and L-Asp decompositions at 433 K (with quenching) are shown in Figure 4 at 10 of the 70 time intervals used in the experiment (see Section SI 6 for the remainder). The extent of reaction (EOR) was used to order the coverage maps. The value of EOR was determined using the average value of the local Asp coverages remaining on the $Cu(111) \pm 14^{\circ}$ -S⁴C after each of the 70 periods of annealing at 433 K, EOR = $1 - \langle \theta_{Asp}^{(hkl)} \rangle$. The orientation of the coverage maps with respect to the highsymmetry directions of the S⁴C is marked on the 0 and 100% EOR maps. The coverage maps reveal a 3-fold rotational symmetry for both Asp enantiomers about the Cu(111) center point, as expected. The Cu(111) orientation is the least reactive in the sense that both Asp enantiomers remain unreacted around the (111) point until EOR approaches 100%. The maps at EOR = 30 and 31% for L- and D-Asp, respectively, show that the decomposition starts at the edges of the crystal where the density of step edges is highest. However, the decomposition kinetics are not isotropic around the edge of the crystal. In particular, the decomposition of L-Asp and D-Asp starts in the S- and R-regions of the surface, respectively, revealing enantiospecificity. For both Asp enantiomers, the (110) step edges are more reactive than the (100) step edges. The patterns at EOR = 30 and 31% show enantiospecificity in the sense that the most reactive regions lie on R- surfaces for D-Asp and on S-surfaces for L-Asp. In contrast with the low EOR maps, the maps at EOR = 47-91% do not reveal noticeable enantiospecificity and show the least reactive regions for both L- and D-Asp being the achiral surfaces with (100) step edges and the surfaces vicinal to the center (111)

One of the interesting features of the decomposition of Asp on Cu(111) is that it decomposes stoichiometrically to H_2 , $2CO_2$, and $N \equiv CCH_3$ without contamination of the surface (Section SI

7). A related experiment has demonstrated that when exposed to a constant flux of Asp, the Cu(111) surface decomposes Asp catalytically and in steady state without apparent deactivation. This could only be possible if the decomposition is stoichiometric and leaves no residue on the Cu(111) surface. Herein, an experiment was conducted in which the clean $Cu(111) \pm 14^{\circ}$ -S⁴C surface at 400 K was saturated with a monolayer of L-Asp that was later decomposed by heating to 600 K. O 1s, C 1s, and N 1s XPS spectra were then collected at 49 points including the (111) center point. The additional 48 points span an angular range of 120° azimuthally from the (100) high-symmetry direction and 12.4° in the polar direction from the center of the $Cu(111) \pm 14^{\circ}-S^{4}C$ to its edge. This corresponds to all possible surface orientations that lie within a polar angle of 12.4° from the $\langle 111 \rangle$ direction. The O 1s, C 1s, and N 1s XPS spectra collected at the 49 points after annealing to decompose the adsorbed monolayer (Section SI 7) show that no detectable C, N, or O remained on the surface after heating to 600 K. This demonstrates that thermal decomposition of adsorbed Asp is stoichiometric on all $Cu(hkl)^{R\&S}$ surfaces vicinal to Cu(111) yielding H₂, 2CO₂, and N≡CCH₃ without contamination of the surface.

4. DISCUSSION

The primary goal of this work has been to map enantiospecific surface reaction rate constants versus surface crystallographic orientation, $k_i^{(hkl)}$ and $k_e^{(hkl)}$, with high enough spatial resolution on the $Cu(111) \pm 14^{\circ}$ -S⁴C to provide insight into the origins of surface structure sensitivity in the decomposition of L- and D-Asp. Estimates of the surface structure dependence of the rate constants $k_i^{(hkl)}$ and $k_e^{(hkl)}$ were obtained from the coverage decay curves for L-Asp and D-Asp decomposition on 169 different Cu(hkl) surfaces vicinal to Cu(111). Greater detail regarding the procedure for $k_i^{(hkl)}$ and $k_e^{(hkl)}$ parameter estimations can be found in prior work on TA decomposition on Cu surfaces.^{8,28} When comparing the L-Asp and D-Asp experiments, small differences in temperature (\sim 1 K) between the experiments may be responsible for differences in the values of EOR achieved after a given time at 433 K. Thus, the value of time used to obtain the rate constants for both L-Asp and D-Asp is the average time to reach a given EOR for both L- and D-Asp, as shown in Section SI 7.

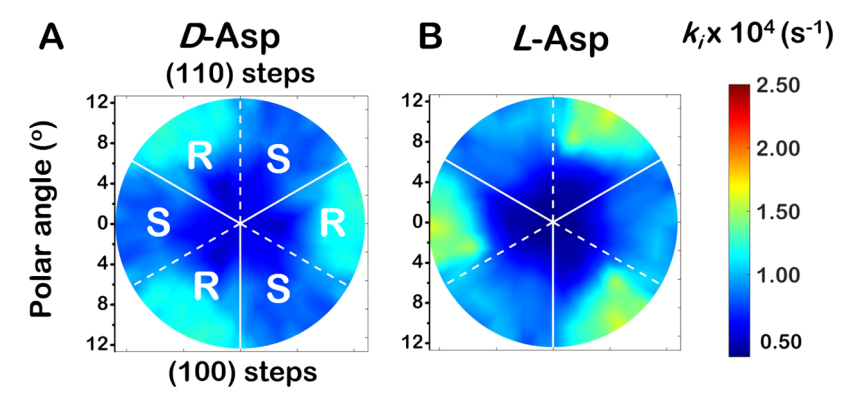


Figure 5. Polar maps of $k_i^{(hkl)}$ for (A) D-Asp and (B) L-Asp decompositions measured at $T_{\rm iso}$ = 433 K across the Cu(111) \pm 14°-S⁴C. The dashed white lines indicate directions exposing (110) steps, and the solid white lines indicate (100) steps. These maps have been rotationally averaged to conform to the 3-fold rotational symmetry of the Cu(111) surface. The raw data prior to rotational averaging can be found in Section SI 9. The ranges of values across the S⁴C are ~3× for both D- and L-Asp. Enantiospecificity in $k_i^{(fikl)}$ is observed in that the values are greatest for D-Asp on the Cu(hkl)⁸ surfaces and greatest for L-Asp on the Cu(hkl)⁸ surfaces.

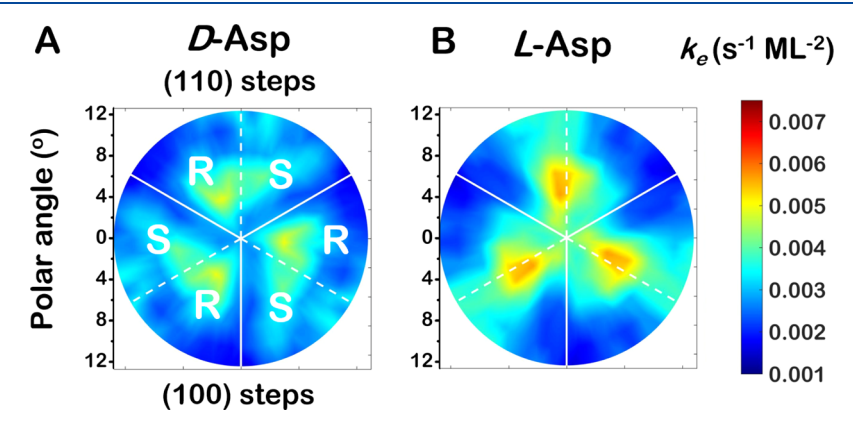


Figure 6. Maps of $k_e^{(hkl)}$ for (A) D-Asp and (B) L-Asp decompositions measured at $T_{\rm iso}$ = 433 K across the Cu(111) \pm 14°-S⁴C. These maps have been rotationally averaged to conform to the 3-fold rotational symmetry of the Cu(111) surface. The ranges of values are ~4× for both D- and L-Asp across the sample. Enantiospecificity in $k_e^{(hkl)}$ is not observed. The maxima and minima in the values of $k_e^{(hkl)}$ lie along the high-symmetry directions.

4.1. Initiation Rate Constant, $k_i^{(hkl)}$, for Asp Decomposition. The rate constants $k_i^{(hkl)}$ and $k_e^{(hkl)}$ for the decomposition of D- and L-Asp on the $Cu(111) \pm 14^{\circ}-S^{4}C$ were estimated by fitting eq 1 to the $\theta_{Asp}^{(hkl)}(t)$ data at each of the 169 surface orientations studied. Figure 5A,B shows the initiation rate constants, $k_i^{(hkl)}$, for D- and L-Asp, respectively, as functions of position on the Cu(111) \pm 14°-S⁴C. The average uncertainty for the values of the initiation rate constants, $k_i^{(hkl)}$, has been determined from the fits of eq 1 to the $\theta_{Asp}^{(hkl)}(t)$ data. The fractional error averaged over all 169 points is ±13% reported with a 95% confidence interval. The values of $k_i^{(hkl)}$ are lowest at the Cu(111) center point where the step density is lowest at the Cu(111) center point where the step county, a lowest. The values of $k_i^{(hkl)}$ are structure-insensitive across the central region of the S⁴C, i.e., within ~9° of the Cu(111) surface. In other words, the values of $k_i^{(hkl)}$ do not reveal any dependence on the azimuthal angle or step orientation around the Cu(111) pole. The $k_i^{(hkl)}$ values are largest from a polar angle of $\sim 9^{\circ}$ to the edge of the sampling region at 12.4° from the (111) direction. More importantly, the values of $k_i^{(hkl)}$ reveal enantiospecificity and are the greatest for D-Asp on the Cu(hkl)R surfaces and greatest for L-Asp on the $Cu(hkl)^S$ surfaces. This is consistent with the initial onset of decomposition for both D- and L-Asp observed in Figure 4 at values of EOR \cong 35%. While Figure 5 reveals clear enantiospecificity of the initiation rate constants, the magnitudes in the high-activity areas at polar angles of $>9^{\circ}$ appear to be slightly higher for L-Asp than for D-Asp, ${}^{L}k_{i}^{(hkl)-S}$ >

 ${}^{\mathrm{D}}k_{i}^{(hkl)-\mathrm{R}}$. In principle, they should be equal on chiral surface orientations related by mirror symmetry. Averaging the ratio of rate constants from symmetry equivalent surface orientations over the surface orientations with polar angles $>8^{\circ}$ yields

 $^{\text{L}}k_i^{(hkl)\text{-S}}/^{\text{D}}k_i^{(hkl)\text{-R}}=1.07\pm0.02$ reported with a 95% confidence interval. This is a small but significant difference in rate constants where ideally there should be none. Our best assessment is that this difference arises from minor differences in the purity of the L-Asp and D-Asp.

Unfortunately, we can only speculate about the origin of the enantiospecificity observed for $k_i^{(hkl)}$. Enantiospecificity is only observed in the regions of high step density at the edges of the sample and, obviously, only in the regions in which the steps expose chiral kinks. It is possible that the packing density of D- or L-Asp on the narrow terraces is reduced by the presence of steps and reduced enantiospecifically by the chirality of the nearby kinks in the step edges. A low packing density for one enantiomer might make it easier for thermal fluctuations in the local packing density to create the vacancies needed to catalyze Asp decomposition via initial decarboxylation.

4.2. Explosion Rate Constant, $k_e^{(hkl)}$, for Asp Decomposition. The rotationally averaged values of the explosion rate constant, $k_e^{(hkl)}$, obtained from the fit of eq 1 to the $\theta_{Asp}^{(hkl)}(t)$ data are shown in Figure 6A,B for D- and L-Asp, respectively. The fractional uncertainty of the values of the explosion rate

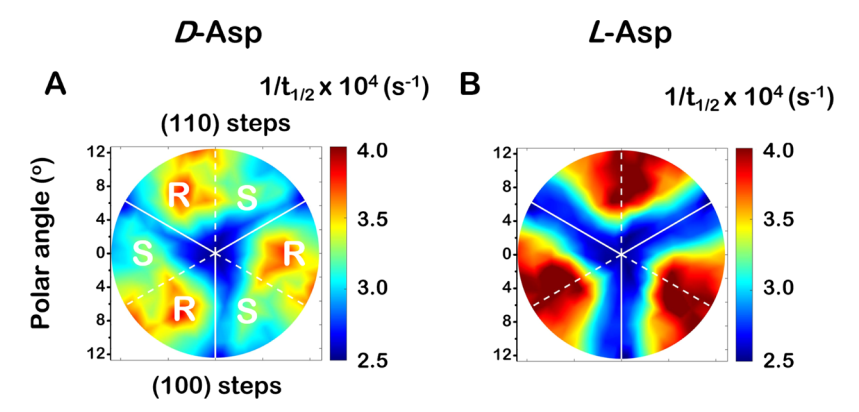


Figure 7. Maps of $t_{1/2}^{-1}$ for (A) D-Asp and (B) L-Asp measured across the Cu(111) \pm 14°-S⁴C. Enantiospecificity in $t_{1/2}^{-1}$ is not observed. The values of $t_{1/2}^{-1}$ are lowest for both D- and L-Asp near the Cu(111) surface and on surface orientations exposing achiral surfaces with (100) steps.

constants averaged over 169 points is ±16% reported with a 95% confidence interval. These maps of $k_e^{(hkl)}$ clearly show structure sensitivity but no obvious sign of enantiospecificity. The values of $k_e^{(hkl)}$ span a range of $\sim 4 \times$ for each Asp enantiomer; however, the regions of highest magnitude straddle the high-symmetry directions exposing achiral surface structures with (110) step edges. The directions along which the values of $k_e^{(hkl)}$ are lowest for both enantiomers are achiral high-symmetry directions exposing surfaces with (100) step edges. It is interesting to note that while the lowest values of $k_e^{(hkl)}$ occur in the low step density region around the (111) point, the maximum values of $k_e^{(hkl)}$ do not occur in the regions having the highest step density at the edges of the crystal. The region with the highest values of $k_e^{(hkl)}$ falls within a polar angle of range $2-8^{\circ}$ from the (111) point and along the directions exposing (110) steps. The low enantiospecificity of $k_e^{(hkl)}$ indicates that the enantiospecificity of $k_i^{(hkl)}$ revealed in Figure 5 is responsible for the enantiospecificity of the Asp decomposition kinetics observed at low values of the EOR in Figure 4. The largest values for $k_e^{(hkl)}$ occur on surfaces with (111) terraces that are ~2.5 nm wide and separated by (110) steps. We note that there appears to be a systematic difference in the magnitudes of the values of ${}^{\text{L}}k_e^{(hkl)-S}$ and ${}^{\text{D}}k_e^{(hkl)-R}$ quantities that are diastereomerically equivalent and ought to be identical. The ratio of rate constants in the region with maximum $k_e^{(hkl)}$ yields ${}^{\text{L}}k_e^{(hkl)-\text{S}}/{}^{\text{D}}k_e^{(hkl)-\text{R}} \approx 1.30 \pm 0.10$. Again, this difference is likely due to a difference in the purities of L-Asp and D-Asp. Sigma-Aldrich specifies the purity of L-Asp and D-Asp as >98% and 99%, respectively. However, their purities were measured differently and the nature of the impurities is not provided making comparison impossible. D-Asp and L-Asp purities were tested by titration and high-performance liquid chromatography (HPLC), respectively.

4.3. Half-Times, $t_{1/2}^{(hkl)}$, for Asp Decomposition. We use the values of $t_{1/2}^{-1}$ as a metric for surface structure-sensitive reaction kinetics because it is based on fundamental kinetic parameters, i.e., the two rate constants, k_i and k_e . As illustrated in Figure 2, the value of $t_{1/2}$ is the time needed for the coverage of Asp to decay from one monolayer initially to $\theta_{\rm Asp}(t_{1/2}) = 0.5$. One can show from the rate law given by eq 1 that $t_{1/2}^{-1} \cong 2\sqrt{k_ik_e}/\pi$. We use $t_{1/2}^{-1}$ rather than $t_{1/2}$ because it has the units of a pseudo-rate constant and is, therefore, easier to compare to k_i and k_e directly. It is also the case that because $t_{1/2}^{-1}$ is the product of k_i and k_e , its value can be estimated more accurately from the data than either k_i or k_e independently. The values of $t_{1/2}^{-1}$ across the Cu(111) \pm 14°-S⁴C are shown in Figure 7A,B for D- and L-Asp, respectively. The uncertainty of the values

of $t_{1/2}^{-1}$ across 169 points is \pm 5% reported with a 95% confidence interval. This is a much lower value than the uncertainty for either k_i or k_e , which means that $t_{1/2}^{-1}$ can be estimated with higher accuracy. The values of $t_{1/2}^{-1}$ range from 2.5×10^{-4} to 4.0×10^{-4} s⁻¹. The regions close to the Cu(111) center of the S⁴C reveal minima in $t_{1/2}^{-1}$ for both enantiomers. Although the ranges of the $t_{1/2}^{-1}$ values for L-Asp and D-Asp are slightly different, they reveal similar trends with respect to surface orientation. For example, the least reactive regions lie on achiral surfaces exposing (100) steps. While surface structure sensitivity is clearly demonstrated, no clear enantiospecificity is observed in the $t_{1/2}^{-1}$ values. In a previous study of D-TA decomposition kinetics on a $Cu(110) \pm$ 14°-S⁴C, enantiospecificity was observed clearly in the $t_{1/2}^{-1}$ values. TA is similar in structure to Asp and decomposes with the same explosion mechanism as Asp on Cu surfaces. ²⁸ For TA decomposition, the values of $k_i^{(hkl)}$ did not reveal enantiospecificity, while the values of $k_e^{(hkl)}$ did reveal enantiospecificity. The values of $t_{1/2}$ for TA decomposition also revealed enantiospecificity that must, in that case, originate from the enantiospecificity of $k_e^{(hkl)}$.

5. CONCLUSIONS

The structure sensitivity and enantiospecificity of the kinetics of D- and L-Asp decompositions on $Cu(hkl)^{R\&S}$ surfaces vicinal to Cu(111) were studied using a $Cu(111) \pm 14^{\circ}$ -S⁴C sample. The kinetics are well described by two rate constants referred to as the initiation rate constant, $k_i^{(hkl)}$, and the explosion rate constant, $k_e^{(hkl)}$, both of which have been estimated from isothermal Asp coverage decay curves, $\theta_{\text{Asp}}^{(hkl)}(t)$, at 169 different surface orientations. Both rate constants reveal clear signs of structure sensitivity exhibiting local minima at the Cu(111) orientation. They both increase with increasing step density but neither isotropically nor monotonically. In the regions of high step density, the values of $k_i^{(hkl)}$ exhibit structure enantiospecificity with ${}^{L}k_i^{(hkl)-S} > {}^{D}k_i^{(hkl)-S}$ and ${}^{D}k_i^{(hkl)-R} > {}^{L}k_i^{(hkl)-R}$. In contrast, the explosion rate constants, $k_e^{(hkl)}$, exhibit structure sensitivity without enantiospecificity. Similarly, the inverse of the half-time, $t_{1/2}^{-1}$ shows clear structure sensitivity without enantiospecificity. It exhibits a minimum at the Cu(111) point and along directions exposing (100) step edges. Along directions exposing (110) step edges, the value of $t_{1/2}^{-1}$ increases monotonically with step density.

ASSOCIATED CONTENT

Supporting Information

The Supporting Information is available free of charge at https://pubs.acs.org/doi/10.1021/acs.jpcc.1c01824.

Graphical illustration of the Cu(3,1,17) chiral surface; stereographic triangle of all possible surface orientations for an FCC lattice; electron backscatter diffraction of the Cu(111) \pm 14°-S 4 C; grid of points used for mapping the coverage of Asp; map and rate constant values for L-Asp decomposition on seven points measured on Cu(111) \pm 14°-S 4 C; data for L- and D-Asp decomposition for all 70 EOR; XPS data for O 1s, C 1s, and N 1s for a monolayer of L-Asp and after annealing at 600 K; heating schedule for L- and D-Asp decomposition on Cu(111) \pm 14°-S 4 C; maps of $k_i^{(hkl)}$, $k_e^{(hkl)}$, and $t_{1/2}^{-1}$ not rotationally averaged (PDF)

AUTHOR INFORMATION

Corresponding Author

Andrew J. Gellman — Department of Chemical Engineering and W.E. Scott Institute for Energy Innovation, Carnegie Mellon University, Pittsburgh, Pennsylvania 15213, United States; orcid.org/0000-0001-6618-7427; Phone: Phone: 1-412-268-3848; Email: gellman@cmu.edu

Author

Carlos Fernández-Cabán — Department of Chemical Engineering, Carnegie Mellon University, Pittsburgh, Pennsylvania 15213, United States

Complete contact information is available at: https://pubs.acs.org/10.1021/acs.jpcc.1c01824

Notes

The authors declare no competing financial interest.

ACKNOWLEDGMENTS

The authors acknowledge support from the NSF under Grant Number CHE1764252.

REFERENCES

- (1) Ertl, G. Reactions at surfaces: From atoms to complexity (Nobel lecture). *Angew. Chem., Int. Ed.* **2008**, 47, 3524–3535.
- (2) Spencer, N. D.; Schoonmaker, R. C.; Somorjai, G. A. Structure sensitivity in the iron single-crystal catalyzed synthesis of ammonia. *Nature* **1981**, *294*, 643–644.
- (3) Gellman, A. J. Chiral Surfaces: Accomplishments and Challenges. *ACS Nano* **2010**, *4*, 5–10.
- (4) Sholl, D. S.; Gellman, A. J. Developing Chiral Surfaces for Enantioselective Chemical Processing. *AIChE J.* **2009**, *55*, 2484–2490.
- (5) Nguyen, L. A.; He, H.; Pham-Huy, C. Chiral drugs: an overview. *Int. J. Biomed. Sci.* **2006**, *2*, 85–100.
- (6) Gellman, A. J.; Tysoe, W. T.; Zaera, F. Surface Chemistry for Enantioselective Catalysis. *Catal. Lett.* **2015**, *145*, 220–232.
- (7) Gellman, A. J.; Ernst, K.-H. Perspective: Chiral autocatalysis and mirror symmetry breaking. *Catal. Lett.* **2018**, *148*, 1610–1621.
- (8) Karagoz, B.; Payne, M.; Reinicker, A.; Kondratyuk, P.; Gellman, A. J. A Most Enantioselective Chiral Surface: Tartaric Acid on All Surfaces Vicinal to Cu(110). *Langmuir* **2019**, *35*, 16438–16443.
- (9) Lawton, T. J.; Pushkarev, V.; Broitman, E.; Reinicker, A.; Sykes, E. C. H.; Gellman, A. J. Initial Oxidation of Cu(hkl) Surfaces Vicinal to Cu(111): A High-Throughput Study of Structure Sensitivity. *J. Phys. Chem. C* 2012, *116*, 16054–16062.
- (10) Prinz, J.; Gröning, O.; Brune, H.; Widmer, R. Highly Enantioselective Adsorption of Small Prochiral Molecules on a Chiral Intermetallic Compound. *Angew. Chem.* **2015**, *127*, 3974–3978.
- (11) Jenkins, S. J. Chirality at Solid Surfaces; John Wiley & Sons, Ltd.: Chichester, U.K., 2018.
- (12) Hazen, R. M.; Sholl, D. S. Chiral selection on inorganic crystalline surfaces. *Nat. Mater.* **2003**, *2*, 367–374.

- (13) McFadden, C. F.; Cremer, P. S.; Gellman, A. J. Adsorption of chiral alcohols on "chiral" metal surfaces. *Langmuir* **1996**, *12*, 2483–2487
- (14) Jenkins, S. J.; Pratt, S. J. Beyond the surface atlas: a roadmap and gazetteer for surface symmetry and structure. *Surf. Sci. Rep.* **2007**, *62*, 373–429.
- (15) Horvath, J. D.; Gellman, A. J. Enantiospecific desorption of chiral compounds from chiral Cu(643) and achiral Cu(111) surfaces. *J. Am. Chem. Soc.* **2002**, *124*, 2384–2392.
- (16) Gellman, A. J.; Huang, Y.; Feng, X.; Pushkarev, V. V.; Holsclaw, B.; Mhatre, B. S. Superenantioselective Chiral Surface Explosions. *J. Am. Chem. Soc.* **2013**, *135*, 19208–19214.
- (17) Yun, Y. J.; Gellman, A. J. Enantioselective Separation on Naturally Chiral Metal Surfaces: d,l-Aspartic Acid on Cu(3,1,17)^{R&S} Surfaces. *Angew. Chem., Int. Ed.* **2013**, *52*, 3394–3397.
- (18) Rampulla, D. M.; Gellman, A. J. Enantioselective decomposition of chiral alkyl bromides on Cu(643)^{R&S}: Effects of moving the chiral center. *Surf. Sci.* **2006**, *600*, 2823–2829.
- (19) Rampulla, D. M.; Francis, A. J.; Knight, K. S.; Gellman, A. J. Enantioselective surface chemistry of R-2-bromobutane on Cu(643)^{R&S} and Cu(531)^{R&S}. *J. Phys. Chem. B* **2006**, *110*, 10411–10420.
- (20) Gellman, A. J.; Huang, Y.; Koritnik, A. J.; Horvath, J. D. Structure-sensitive enantiospecific adsorption on naturally chiral Cu(hkl)^{R&S} surfaces. *J. Phys.: Condens. Matter* **2017**, 29, No. 034001.
- (21) de Alwis, A.; Holsclaw, B.; Pushkarev, V. V.; Reinicker, A.; Lawton, T. J.; Blecher, M. E.; Sykes, E. C. H.; Gellman, A. J. Surface Structure Spread Single Crystals (S⁴Cs): Preparation and characterization. *Surf. Sci.* **2013**, *608*, 80–87.
- (22) Mhatre, B. S.; Dutta, S.; Reinicker, A.; Karagoz, B.; Gellman, A. J. Explosive enantiospecific decomposition of aspartic acid on Cu surfaces. *Chem. Commun.* **2016**, *52*, 14125–14128.
- (23) Yun, Y.; Kondratyuk, P.; Gellman, A. J. Steady-state catalytic decomposition of aspartic acid on Cu(111). *J. Phys. Chem. C* **2019**, *123*, 7594–7603.
- (24) Karagoz, B.; Reinicker, A.; Gellman, A. J. Kinetics and mechanism of aspartic acid adsorption and its explosive decomposition on Cu(100). *Langmuir* **2019**, *35*, 2925–2933.
- (25) Falconer, J.; McCarty, J.; Madix, R. J. The Explosive Decomposition of Formic Acid on Clean Ni(110). *Jpn. J. Appl. Phys.* **1974**, *13*, No. 525.
- (26) Mhatre, B. S.; Pushkarev, V.; Holsclaw, B.; Lawton, T. J.; Sykes, E. C. H.; Gellman, A. J. A Window on Surface Explosions: Tartaric Acid on Cu(110). *J. Phys. Chem. C* 2013, *117*, 7577—7588.
- (27) Benziger, J. B.; Madix, R. J. Decomposition of formic-acid on Ni(100). Surf. Sci. 1979, 79, 394–412.
- (28) Kondratyuk, P.; Karagoz, B.; Yun, Y. J.; Gellman, A. J. Initiation of Vacancy-Mediated, Surface Explosion Reactions: Tartaric and Aspartic Acid on Cu Surfaces. *J. Phys. Chem. C* **2019**, *123*, 18978—18985.